Fusion-based Variational Image Dehazing

Adrian Galdran, Javier Vazquez-Corral, David Pardo, and Marcelo Bertalmío,

***Abstract*—We propose a novel image dehazing technique based on the minimization of two energy functionals and a fusion scheme to combine the output of both optimizations. The proposed Fusion-based Variational Image Dehazing method (FVID) is a spatially varying image enhancement process that proceeds by first minimizing a previously proposed variational formulation that maximizes contrast and saturation on the hazy input. The iterates produced by this minimization are kept, and a second energy that tends to shrink faster the intensity values of well-contrasted regions is minimized, allowing to generate a set of Difference-of-Saturations (DiffSat) maps by observing the shrinking rate. The iterates produced in the first minimization are then fused with these DiffSat maps to produce a haze-free version of the degraded input. The FVID method does not rely on a physical model from which to estimate a depth map, nor it needs a training stage on a database of human-labelled examples. Experimental results on a wide set of hazy images demonstrate that FVID better preserves the image structure on close-by regions that are less affected by fog, and it successfully compares with other current methods in the task of removing haze degradation from far-away regions.**

***Index Terms*—Image Dehazing, Variational Image Processing, Image Fusion, Color Correction, Contrast Enhancement.**

September 8, 2016

I. Introduction

IMAGES acquired in outdoor scenarios often suffer from a particular kind of degradation produced by the atmosphere that lies between the observer and objects in the scene. This phenomenon, usually referred to as haze or fog, distorts contrast and color in the image, decreasing the visibility of the contents of the scene and reducing its visual quality.

The task of removing haze degradation from an image is known as image dehazing, and has given rise to an important area of research recently. A first family of methods rely on inverting a physical model of the degradation, such as Koschmieder's atmospheric scattering model [1]:

$$\mathrm{I}(x) = \mathrm{t}(x)\mathrm{J}(x) + (1 - \mathrm{t}(x))\mathrm{A}. \tag{1}$$

Here, x represents a pixel location, $\mathrm{I}(x)$ is the observed intensity, $\mathrm{J}(x)$ is the scene radiance of a haze-free image, $\mathrm{t}(x)$ is the transmission of light in the atmosphere, inversely related to the scene's depth, and A is the airlight, a global vector quantity describing the ambient light.

Whenever no extra information apart from the input image is considered, the problem is known as single-image dehazing. The first approach to tackle the problem is to formulate some restriction on the visual characteristics that a reasonable solution can have, see [2]–[4]. In particular, the most popular work is the Dark Channel Prior [5], which states that haze-free images locally have a low value of luminance in some of the three color channels. Extensions of this cue have been further used in[6]–[12]. A second type of approaches to image dehazing is that of machine-learning techniques. Relevant works are [10], [13]–[15]. A third group of methods are based on spatially varying image processing techniques. They study the local structure of the image to infer the presence of haze, and try to compensate for this effect, see for instance [16] or[17]. Fusion of white balanced and contrast enhanced versions of the input hazy image has also been proposed [18], as well as approaches based on models of the Human Visual System, such as Retinex,[19]–[21]. The main drawback of these methods is that, due to the partial lack of physical information within their formulation, they may present under or overenhanced results, see Fig. (1). In general, a well-designed image dehazing method should strive to enhance visibility in areas of the scene lying far away from the observer, but regions not affected by fog should keep their original luminance and chromatic characteristics.

The main contribution in this paper is the development of a variational dehazing method that improves previous works by retaining high contrast and colourfulness enhancing capabilities on far away regions, while preserving image content on nearby regions. This is made possible through a double minimization: we optimize a first energy to generate a series of Difference-of-Saturations maps that encode the degree of degradation of each pixel in the scene. Then, a second energy is combined with the previously derived maps to recover haze-free images.

II. Variational image dehazing

To restore haze-degraded outdoor images, in [22], the authors proposed to minimize the following image energy:

$$\begin{aligned}\mathrm{E}_{\mathrm{EVID}}(\mathrm{I}^j) = &\frac{\alpha}{2}\sum_x (\mathrm{I}^j(x) - \mu^j)^2 + \frac{\beta}{2}\sum_x (\mathrm{I}^j(x) - \mathrm{I}_0^j(x))^2 \\ &- \frac{\gamma}{2}\sum_{x,y}\omega(x,y)|\mathrm{I}^j(x) - \mathrm{I}^j(y)| - \frac{\eta}{2}\sum_{x,y}\omega(x,y)|\mathrm{I}^j(x) - \mathrm{I}^{j+1}(y)| \\ &- \frac{\eta}{2}\sum_{x,y}\omega(x,y)|\mathrm{I}^j(x) - \mathrm{I}^{j+2}(y)|,\end{aligned} \tag{2}$$

where I^j is a color channel with values in $[0,1]$, I_0 is the original image, x, y are pixel coordinates, $\alpha, \beta, \gamma, \eta$ are positive parameters, and $\omega(x,y)$ is a distance function with values decreasing as the distance between x and y increases, $\mu^j \approx$

A. Galdran is with Tecnalia, Computer Vision Group, E-48160, Derio, Spain (e-mail: adrian.galdran@tecnalia.com). J. Vazquez-Corral and M. Bertalmio are with Universitat Pompeu Fabra, E-08018, Barcelona, Spain (e-mails: {javier.vazquez, marcelo.bertalmio}@upf.edu). They are supported by the ERC, Starting Grant ref. 306337, the Spanish government, grant ref. TIN2015-71537-P, and the ICREA Academia Award. D. Pardo is with University of the Basque Country (UPV/EHU), E-48940, Leioa, Spain; the Basque Center for Applied Mathematics (BCAM), E-48009, Bilbao, Spain; and Ikerbasque, Basque Foundation for Science, Bilbao, Spain. (e-mail: dzubiaur@gmail.com). He iss funded by the Spanish government, grant ref. MTM2013-40824-P, the BCAM Severo Ochoa accreditation of excellence SEV-2013-0323, and the Basque Government Consolidated Research Group Grant IT649-13.

Manuscript received May 15, 2016; revised June 26, 2016.

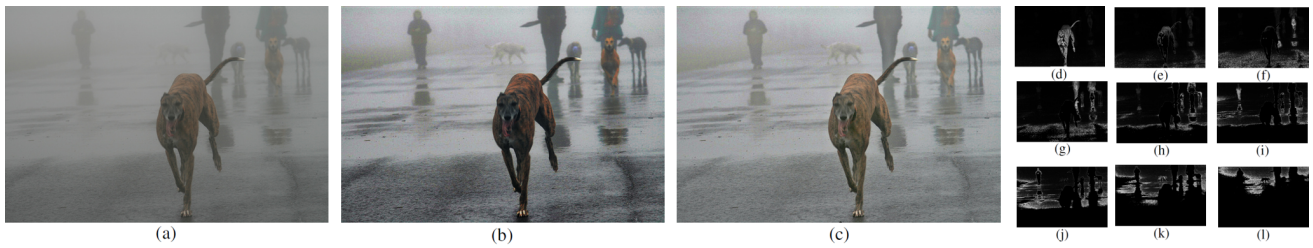

Fig. 1. (a) A hazy scene, and the result of applying (b) EVID dehazing technique (c) The proposed FVID method. (d)-(l) The progressive DiffSat maps generated by our approach. Note the loss of details in the face of the dog produced by EVID. This overenhancement artifact is properly corrected by FVID.

$2\ \mathrm{mean}(\mathrm{I}^j) - \mathrm{A}^j$ is a mechanism to estimate the predicted mean of the haze-free image, and $j \in \mathbb{Z}_3$. Here, $\{R, G, B\}$ is identified with the space of integers modulo 3, $\mathbb{Z}_3$, meaning for instance that $\mathrm{I}^2 = \mathrm{I}^G$, and $\mathrm{I}^3 = \mathrm{I}^B$. This energy is termed Enhanced Variational Image Dehazing (EVID).

III. Fusion-based variational image dehazing

Despite the good dehazing capabilities of the method described by (2), it sometimes produces overenhanced results, see fig. 1. Still, each of the iterates generated by EVID implicitly carries useful information on the degree of enhancement each region needs. This observation leads us to design a methodology that extracts such information, in the form of progressive Difference-of-Saturations (DiffSat) maps. After building these maps, we use them to formulate an image fusion process to blend the EVID iterates into a single image, keeping only the most useful visual information at each depth layer of the hazy input.

A. Progressive DiffSat Maps Generation

To capture the implicit depth information that EVID generates, we extend the energy of (2) as follows:

$$\mathrm{E}_{\mathrm{FVID}}(\mathrm{I}^j) = \mathrm{E}_{\mathrm{EVID}}(\mathrm{I}^j) + \tau \sum_x \mathrm{I}^j(x). \tag{3}$$

This straightforward extension keeps the dehazing capabilities of EVID, but it adds a penalty term for large image intensity values. In practice, this amounts to prioritizing a dark image.

To minimize the $\mathrm{E}_{\mathrm{FVID}}$ energy, we compute the Euler-Lagrange equations by means of the following theorem:

Theorem 1. *For the* $\mathrm{E}_{\mathrm{FVID}}$ *energy, the Euler-Lagrange equations are:*

$$\begin{aligned}\nabla \mathrm{E}_{\mathrm{FVID}}(\mathrm{I}^j) =& \alpha(\mathrm{I}^j - \mu_j) + \beta(\mathrm{I}^j - \mathrm{I}_0^j) - \gamma R(\mathrm{I}^j, \mathrm{I}^j) \\ & -\eta(R(\mathrm{I}^j, \mathrm{I}^{j+1}) + R(\mathrm{I}^j, \mathrm{I}^{j+2})) + \tau = 0 \end{aligned} \tag{4}$$

for $j \in \{R, G, B\}$. *Here,* $R(\mathrm{I}^i, \mathrm{I}^j)$ *is defined as follows:*

$$R(\mathrm{I}^i, \mathrm{I}^j)(x) = \frac{\sum_y \omega(x,y) s(\mathrm{I}^i(x) - \mathrm{I}^j(y))}{\sum_y \omega(x,y)}, \tag{5}$$

being s *a sigmoid function, and with* j *defined modulo* 3, *varying in the* $\{R, G, B\}$ *components of the input image.*

Proof. The variational derivatives of the modified gray-world term, the attachment to data term, and shrinking term are straightforward to compute. The contrast and the saturation enhancement terms need a more tedious computation, the details of which can be found in [22]. □

Once the gradient of the energy is computed, we can advance towards a minimum of it by using gradient descent:

$$\begin{aligned}\mathrm{I}_{k+1}^j =& \mathrm{I}_k^j(1 - \Delta t(\alpha + \beta)) + \Delta t(\alpha \mu^j + \beta \mathrm{I}_0) \\ &+ \Delta t[\gamma R(\mathrm{I}_k^j, \mathrm{I}_k^j) + \eta[R(\mathrm{I}_k^j, \mathrm{I}_k^{j+1}) + R(\mathrm{I}_k^j, \mathrm{I}_k^{j+2})] - \tau]. \end{aligned} \tag{6}$$

The additional term inserted in (3) penalizes large intensity values in the image. Thus, the above gradient descent will shrink intensity values of the hazy input image. Note that we minimize the energy in the space of images with non-negative values. This imposes a non-linear constraint that can be handled with different approaches, e.g. introducing the KKT conditions [23]. A simpler approach employed in this work consists of, whenever an iteration takes a negative value, back-projecting the image again into the $[0, 1]$ space.

Note that the minimization of $\mathrm{E}_{\mathrm{FVID}}$ differs from the minimization of $\mathrm{E}_{\mathrm{EVID}}$ in that we introduce a shift in the Gray-World value. To see this, we may reformulate (4) as:

$$\begin{aligned}\nabla \mathrm{E}_{\mathrm{FVID}}(\mathrm{I}^j) =& \alpha\left(\mathrm{I}^j - (\mu_j - \frac{\tau}{\alpha})\right) + \beta(\mathrm{I}^j - \mathrm{I}_0^j) \\ &- \gamma R(\mathrm{I}^j, \mathrm{I}^j) - \eta(R(\mathrm{I}^j, \mathrm{I}^{j+1} + R(\mathrm{I}^j, \mathrm{I}^{j+2})) = 0. \end{aligned} \tag{7}$$

Thus, to enforce a dark image as the minimum of $\mathrm{E}_{\mathrm{FVID}}$, we need to impose that $\mu_j \leq \tau/\alpha$, for every color channel j. This amounts to require $2\ \cdot \mathrm{mean}(\mathrm{I}^j) - \mathrm{A}^j \leq \tau/\alpha$. Once this condition is fulfilled, and given the local nature of the contrast and saturation terms, whenever intensities within a region take zero values during the gradient descent, those terms do not contribute to the image energy. In that way, the minimum of the $\mathrm{E}_{\mathrm{FVID}}$ energy will be attained at a black image.

Nevertheless, we are not interested in the minimum of (3), but in the rate at which intensity values of individual pixels $\mathrm{I}(x, y)$ reach zero value. Closer regions have more saturated pixels, and their value rapidly decrease driven by the inter-channel contrast maximization. Far-away regions contain mostly achromatic, non-saturated pixels, that will take more time to vanish. This observation leads us to observe the difference in saturation of each iteration with respect to the previous one. Thus, we generate a series of Difference-of-Saturations (DiffSat) maps to accurately reflect the depth distribution in the scene:

$$\mathrm{D}_k = \mathrm{Sat}(\mathrm{I}_k) - \mathrm{Sat}(\mathrm{I}_{k-1}), \tag{8}$$

where I_k are the iterations generated by (6), and $\mathrm{Sat}(\mathrm{I}_k)$ is the saturation of I_k as defined in eq. (1.73) on [24], being $\mathrm{I}_0 = \mathrm{I}$

the hazy input. An illustration of the generated DiffSat maps is shown in figs. (1.d) - (1.l).

B. Fusion Procedure

We have obtained a set of k depth maps D_k that indicate the amount and location of the haze to be removed at each iteration. We have also obtained a series of l progressively haze-free iterates $\mathcal{I}_l$. Our goal now is to fuse these two sets of information so that depth maps corresponding to later iterates, i.e. those regions with higher fog, should correlate with further processed haze-free iterations.

First, we either interpolate or extrapolate the set of depth maps $\{\mathrm{D}_k\}$ to obtain a new set of exactly l depth maps. These new maps are convolved with a Gaussian kernel in the three dimensions (x,y, and temporal) in order to present smoothed transitions, and they are later normalized so that the sum in the temporal dimension for any pixel x is equal to 1. We will denote these new maps as $\{\mathcal{D}_l\}$.

We compute the fused image as the combination of these normalized depth maps and the haze-free iterates as follows

$$\mathrm{FVID}(x) = \sum_{j=1}^{l} \mathcal{D}_j(x) \cdot \mathcal{I}_j(x)^{\Gamma_j} \tag{9}$$

where $\Gamma = [\Gamma_1, \cdots, \Gamma_l]$ is a set of increasing values between 0.45 and 1.2 that counter-effects the fact that the original image is in linear form (i.e. it is not gamma corrected).

IV. Experimental Evaluation

We implement (2) and (3) with the following reference values: $\alpha = 0.5$, $\beta = 0.5$, $\gamma = 0.2$, $\eta = 0.02$ and $\tau = 1$. Note that the first four parameters keep the same values as in the original EVID formulation [22]. The parameter τ is chosen in such a way that condition $\mu_j \leq \tau/\alpha$ is fulfilled. For the above values of α and τ, $\tau/\alpha = 2 \geq 2\,\mathrm{mean}(\mathrm{I}^j) - \mathrm{A}^j$, since $0 \leq \mathrm{I}^j, \mathrm{A}^j \leq 1$ for all j. Both distance functions were defined as Gaussians with a kernel of standard deviation 50 pixels. The time step was set to $\Delta t = 0.15$ for (2) and $\Delta t = 0.05$ for (3), to allow for a more fine-grained DiffSat map set. We consider that a steady-state of the gradient descent is achieved when the difference between the images of two consecutive iterations is below 0.02. The set of Γ values for (9) is equally spaced between the 0.45 value considered for the first iterate and the 1.2 value employed for the last one.

Regarding efficiency, variational models are often both powerful and computationally demanding. In this case, FVID doubles the computational complexity of EVID, since we need to minimize model (2) first, and model (3) afterwards to generate the iterates and the maps, in order to perform the fusion. Fortunately, the same technique, based on FFT, that was proposed in [25] ,can be applied in both cases, rendering a computation time of about 90 seconds for a 1 MP image.

Fig. 2 describes a foggy scene that is often employed to evaluate the performance of dehazing approaches. We can conclude that, while every tested method improves visibility of the wheat piles at the bottom of the scene, the method in [4] and EVID suffer from a heavy overenhancing that leads to the appearance of distorted artificial colors. In this case, the remaining techniques, i.e., the approaches proposed in [3], [6] and FVID, seem to recover a satisfactory dehazed result. We confirm this by conducting a simple experiment. First, we obtain a depth map by applying the popular Dark Channel method, which provides a reliable transmission map for images degraded by homogeneous fog. After re-scaling the transmission to the $[0, 1]$ interval, we threshold it in successive percentages of depth, obtaining a series of cumulative depth maps and corresponding partial images, see figs. (3.b) to (3.e). For each thresholded depth map, we measure the deviation of the original image with respect to the dehazed result provided by each of the methods, in terms of image structure. To that end, we apply the well-known SSIM index [26].

Results of this experiment applied to the wheat field image in fig. 2 are presented in fig. 3. We see that every dehazing method produces a decreasing sequence of SSIM scores, as expected. As we progressively add further regions of the image to the error analysis, the similarity of the original image and the dehazed output decreases. However, we can observe that the method of [4] and EVID produce rapidly decreasing scores. This means that, in the effort of dehazing far-away areas, both methods aggressively modify nearby regions. This is visually confirmed by the clearly overenhanced results of figs. (3.b) and (3.e). On the other hand, the methods of [3], [6] and FVID produce more balanced successive SSIM scores, *i.e.*, they better preserve nearby areas. While far-away areas of the scene seem to be satisfactorily dehazed by all the methods, the FVID approach produces a dehazed image that slowly separates from the input hazy scene, succeeding in dehazing the scene progressively while better keeping the structural similarity with respect to the less hazy parts of the image.

One of the nice features of EVID is its capability to dehaze images even when they contain an uneven source of illumination. We demonstrate that FVID preserves this capability in fig. 4, a natural image where the sun illuminates objects from the left of the scene, providing a non-uniform illumination. As usual in dehazing methods that assume a regular spatial distribution of haze, the techniques proposed in [3], [5], [15] overcompensate the illumination in the left part of the image, introducing yellowish artificial tones. In contrast, we can observe how both EVID and FVID retrieve visibility to a similar degree (see the central tree), while not introducing the color artifacts induced by the sun behind the haze. It is also noticeable how EVID produces excessive contrast on nearby regions, as observed in the areas of grass close to the camera. These specific artifacts are satisfactorily avoided by FVID.

Another important problem that current dehazing approaches seldom address [27] is the appearance of chromatic artifacts when processing sky regions. Due to their low saturation, sky pixels tend to confound depth estimation algorithms, which classify them as being contaminated by haze, and attempt to extract too much contrast. This problem is exacerbated by the reduction of information that compression algorithms often apply to those regions [28]. In our case, we can take advantage of the flexibility of the variational approach to process sky areas on the image without introducing overenhancing artifacts. To this end, we consider an adaptive weighting strategy for

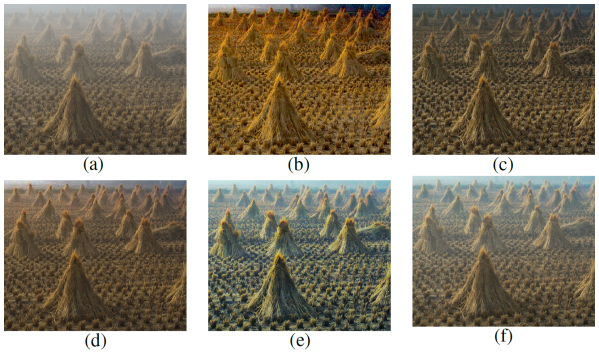

Fig. 2. A hazy scene and the output of different dehazing methods. (a) Original scene. (b) Bayesian defogging [4] (c) No-black-pixel [3] (d) BCCRD [6] (e) EVID [22] (f) FVID.

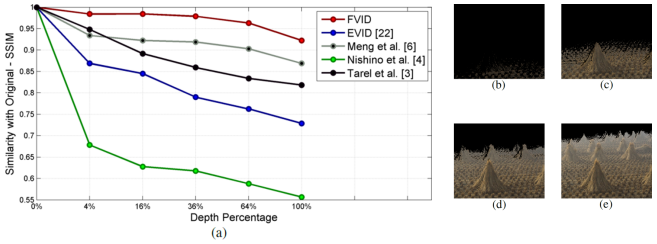

Fig. 3. SSIM of the progressive partial images produced masking the dehazed outputs of fig. (2) by binarized depth maps. Figs. (b)-(e) show progressive masked images at a depth of: (b) 4% (c) 16% (d) 36% (e) 64%.

the attachment to data term in the DiffSat map generation scheme. In particular, when we apply FVID to a hazy image with sky region on it, we modify β in (3) simply to be an array of increasing weights, $\beta = (\beta_i) = (\beta_0 \cdot 1.1^i)$. This produces a set of DiffSat maps that do not consider sky regions as being far away, and leads to a more conservative behaviour of the fusion stage therein. An example of this approach is shown in fig. 5, where we compare it versus the result of the standard FVID, as well as EVID and the Dark Channel [5] and FADE [15] methods, to better appreciate the artifact removal effect of the adaptive attachment-to-data term. We can see how the chromatic distortion generated by standard FVID on sky regions is mitigated by this modified version, while contrast gain is retained in other areas of the image, such as far-away buildings. We have zoomed in the sky region to better notice the presence of these distortions, that is substantially alleviated with the proposed adaptive attachment-to-data strategy.

To quantitatively evaluate FVID we perform a similar evaluation procedure as in [22]. Our evaluation dataset it is composed of 48 foggy images: 12 scenes from [29] under 4 different realistic fog layers. We have compared FVID versus other state-of-the-art methods, namely EVID [22], and the methods proposed in [5], [3], and [30]. Again, our method was computed with the same fixed parameters for all scenes.

In this paper, we slightly modify the 5 image metrics used in [22]. Here, the first measure computes the peak-signal-to-noise ratio (PSNR) between each channel of the images to later combine the results of the three channels using the l_2 norm, that is $\text{PSNR}_{split} = \sqrt{\sum_{c=r,g,b} \text{PSNR}(I_c^{GT}, I_c^m)^2}$,

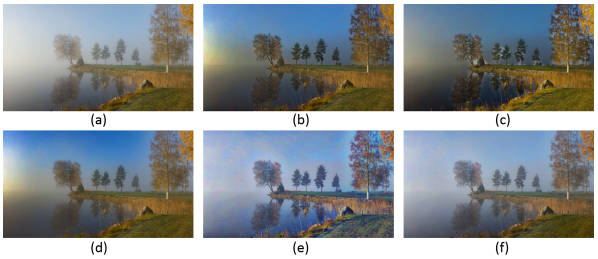

Fig. 4. A hazy scene suffering from an uneven illumination and the output of different dehazing methods. (a) Original hazy scene. (b) FADE [15] (c) No-black pixel [3] (d) Dark channel [5] (e) EVID [22] (f) FVID.

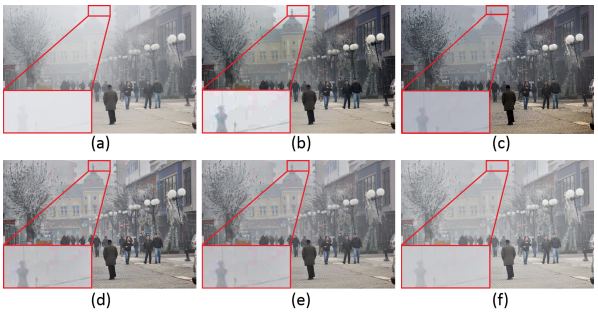

Fig. 5. A hazy image with a reduced sky region, and the result of dehazing it with: (b) Dark channel [5] (c) FADE [15] (d) EVID (e) FVID (f) FVID with adaptive attachment to data term.

where I^{GT} stands for the ground-truth image, I^m stands for the method used, the subindexes represent each color channel. The second measure is the PSNR between the luminance of the images. The third measure is called $l2-color$ and computed as $l_2 - color = \frac{\sum_{i=1}^{M} \sqrt{\sum_{c=r,g,b} (I_c^{GT}(i) - I_c^m(i))^2}}{M}$, where the images are considered in the range (0,255). The last two measures are based on the correlation. They are mathematically defined as $\text{Corr}_{split} = \sqrt{\sum_{c=r,g,b} \text{Corr}(I_c^{GT}, I_c^m)^2}$, and $\text{Corr}_{lum} = \text{Corr}(I_{lum}^{GT}, I_{lum}^m)$, where Corr gives us the correlation coefficient between the two images. Results are shown in Table I. For all the evaluated measures, except for the $l2-color$, a higher value means a better method. The FVID method proposed in this paper outperforms all the others.

TABLE I
QUANTITATIVE RESULTS AS THE MEAN FOR 48 IMAGES

Error measure	[30]	[3]	[5]	EVID [22]	FVID
l2-color	47.96	52.03	48.93	47.18	**44.42**
$PSNR_{lum}$	16.03	16.52	15.53	17.00	**17.31**
$PSNR_{split}$	6.90	6.99	6.79	7.13	**7.19**
$Corr_{split}$	1.24	1.21	1.18	1.25	**1.26**
$Corr_{lum}$	0.70	0.69	0.66	0.71	**0.72**

V. Discussion and Conclusions

We have described FVID, a novel haze removal method. It extends significantly upon a previously proposed variational dehazing scheme (EVID) through a double optimization that integrates information of the iterates produced by EVID and a hierarchical set of partial depth estimates, obtained from

a simple extension of the EVID image energy. The fusion of visual information coming from both sources leads to an effective dehazing technique that is validated through experimental evaluation. FVID achieves results comparable to other state-of-the-art techniques in the task of enhancing contrast of colors of far-away regions, while better retaining image structure in nearby regions. As a side contribution, we have also proposed a variant of FVID to handle typical overenhancement artifacts that often appear when dehazing images containing sky regions. Moreover, and due to the flexibility of variational minimization methods, it is possible to generate different families of FVID methods exhibiting different features, which shall be explored in future works.

REFERENCES

[1] H. Koschmieder, *Theorie der horizontalen Sichtweite: Kontrast und Sichtweite*. Keim & Nemnich, 1925.

[2] R. Fattal, "Single Image Dehazing," in *ACM SIGGRAPH 2008 Papers*, ser. SIGGRAPH '08. New York, NY, USA: ACM, 2008, pp. 72:1–72:9.

[3] J. P. Tarel and N. Hautiere, "Fast visibility restoration from a single color or gray level image," in *2009 IEEE 12th International Conference on Computer Vision (ICCV)*, Sep. 2009, pp. 2201–2208.

[4] K. Nishino, L. Kratz, and S. Lombardi, "Bayesian Defogging," *International Journal of Computer Vision*, vol. 98, no. 3, pp. 263–278, Jul. 2012.

[5] K. He, J. Sun, and X. Tang, "Single Image Haze Removal Using Dark Channel Prior," *IEEE Transactions on Pattern Analysis and Machine Intelligence*, vol. 33, no. 12, pp. 2341–2353, Dec. 2011.

[6] G. Meng, Y. Wang, J. Duan, S. Xiang, and C. Pan, "Efficient Image Dehazing with Boundary Constraint and Contextual Regularization," in *2013 IEEE International Conference on Computer Vision (ICCV)*, Dec. 2013, pp. 617–624.

[7] W. Sun, "A new single-image fog removal algorithm based on physical model," *Optik - International Journal for Light and Electron Optics*, vol. 124, no. 21, pp. 4770–4775, Nov. 2013.

[8] Y. Gao, H.-M. Hu, S. Wang, and B. Li, "A fast image dehazing algorithm based on negative correction," *Signal Processing*, vol. 103, pp. 380–398, Oct. 2014.

[9] J.-B. Wang, N. He, L.-L. Zhang, and K. Lu, "Single image dehazing with a physical model and dark channel prior," *Neurocomputing*, vol. 149, Part B, pp. 718–728, Feb. 2015.

[10] Q. Zhu, J. Mai, and L. Shao, "A Fast Single Image Haze Removal Algorithm Using Color Attenuation Prior," *IEEE Transactions on Image Processing*, vol. 24, no. 11, pp. 3522–3533, Nov. 2015.

[11] Z. Li and J. Zheng, "Edge-Preserving Decomposition-Based Single Image Haze Removal," *IEEE Transactions on Image Processing*, vol. 24, no. 12, pp. 5432–5441, Dec. 2015.

[12] Y.-H. Lai, Y.-L. Chen, C.-J. Chiou, and C.-T. Hsu, "Single-Image Dehazing via Optimal Transmission Map Under Scene Priors," *IEEE Transactions on Circuits and Systems for Video Technology*, vol. 25, no. 1, pp. 1–14, Jan. 2015.

[13] K. Tang, J. Yang, and J. Wang, "Investigating Haze-Relevant Features in a Learning Framework for Image Dehazing," in *2014 IEEE Conference on Computer Vision and Pattern Recognition (CVPR)*, Jun. 2014, pp. 2995–3002.

[14] B. Cai, X. Xu, K. Jia, C. Qing, and D. Tao, "DehazeNet: An End-to-End System for Single Image Haze Removal," *arXiv:1601.07661*, Jan. 2016. [Online]. Available: http://arxiv.org/abs/1601.07661

[15] L. K. Choi, J. You, and A. C. Bovik, "Referenceless Prediction of Perceptual Fog Density and Perceptual Image Defogging," *IEEE Transactions on Image Processing*, vol. 24, no. 11, pp. 3888–3901, Nov. 2015.

[16] R. Tan, "Visibility in bad weather from a single image," in *2008 IEEE Conference on Computer Vision and Pattern Recognition (CVPR)*, Jun. 2008, pp. 1–8.

[17] J. Oakley and H. Bu, "Correction of Simple Contrast Loss in Color Images," *IEEE Transactions on Image Processing*, vol. 16, no. 2, pp. 511–522, Feb. 2007.

[18] C. Ancuti and C. Ancuti, "Single Image Dehazing by Multi-Scale Fusion," *IEEE Transactions on Image Processing*, vol. 22, no. 8, pp. 3271–3282, Aug. 2013.

[19] V. De Dravo and J. Hardeberg, "Stress for dehazing," in *Colour and Visual Computing Symposium (CVCS), 2015*, Aug. 2015, pp. 1–6.

[20] X.-S. Zhang, S.-B. Gao, C.-Y. Li, and Y.-J. Li, "A Retina Inspired Model for Enhancing Visibility of Hazy Images," *Frontiers in Computational Neuroscience*, p. 151, 2015.

[21] Y. Wang, H. Wang, C. Yin, and M. Dai, "Biologically inspired image enhancement based on Retinex," *Neurocomputing*, vol. 177, pp. 373–384, Feb. 2016.

[22] A. Galdran, J. Vazquez-Corral, D. Pardo, and M. Bertalio, "Enhanced Variational Image Dehazing," *SIAM Journal on Imaging Sciences*, vol. 8, no. 3, pp. 1519–1546, Jan. 2015.

[23] J.-B. Hiriart-Urruty and C. Lemaréchal, *Convex Analysis and Minimization Algorithms I*, M. Artin, S. S. Chern, J. Coates, J. M. Fröhlich, H. Hironaka, F. Hirzebruch, L. Hörmander, C. C. Moore, J. K. Moser, M. Nagata, W. Schmidt, D. S. Scott, Y. G. Sinai, J. Tits, M. Waldschmidt, S. Watanabe, M. Berger, B. Eckmann, and S. R. S. Varadhan, Eds. Berlin, Heidelberg: Springer Berlin Heidelberg, 1993.

[24] K. N. Plataniotis and A. N. Venetsanopoulos, *Color Image Processing and Applications*, ser. Digital Signal Processing, A. Lacroix and A. N. Venetsanopoulos, Eds. Berlin, Heidelberg: Springer Berlin Heidelberg, 2000. [Online]. Available: http://link.springer.com/10.1007/978-3-662-04186-4

[25] M. Bertalio, V. Caselles, E. Provenzi, and A. Rizzi, "Perceptual color correction through variational techniques," *IEEE Transactions on Image Processing*, vol. 16, no. 4, pp. 1058–1072, Apr. 2007.

[26] Z. Wang, A. Bovik, H. Sheikh, and E. Simoncelli, "Image quality assessment: From error visibility to structural similarity," *IEEE Transactions on Image Processing*, vol. 13, no. 4, pp. 600–612, Apr. 2004.

[27] Y.-b. Zhu, J.-m. Liu, and Y.-g. Hao, "A single image dehazing algorithm using sky detection and segmentation," in *2014 7th International Congress on Image and Signal Processing (CISP)*, Oct. 2014, pp. 248–252.

[28] Y. Li, F. Guo, R. T. Tan, and M. S. Brown, "A Contrast Enhancement Framework with JPEG Artifacts Suppression," in *Computer Vision –ECCV 2014*, ser. Lecture Notes in Computer Science, D. Fleet, T. Pajdla, B. Schiele, and T. Tuytelaars, Eds. Springer International Publishing, Sep. 2014, no. 8690, pp. 174–188.

[29] C.-C. Su, L. Cormack, and A. Bovik, "Color and Depth Priors in Natural Images," *IEEE Transactions on Image Processing*, vol. 22, no. 6, pp. 2259–2274, Jun. 2013.

[30] K. Gibson and T. Nguyen, "Fast single image fog removal using the adaptive Wiener filter," in *2013 20th IEEE International Conference on Image Processing (ICIP)*, Sep. 2013, pp. 714–718.